# Ultrafast Sorting: Excimeric π-π Stacking Distinguishes Pyrene-*N*-methylacetamides Isomers on the Ultrafast Time Scale.

Krishnayan Basuroy,*[a] Jose de J. Velazquez-Garcia,[a] Darina Storozhuk,[a] David J. Gosztola,[b] Sreevidya Thekku Veedu[a] and Simone Techert*[ac]

[a)]*Deutsches Elektronen-Synchrotron DESY, Notkestr. 85, 22607 Hamburg, Germany.*
[b)]*Center for Nanoscale Materials, Argonne National Laboratory, Lemont, Illinois 60439, United States.*
[c)]*Institute of X-ray Physics, University of Göttingen, Friedrich-Hund-Platz 1, 37077 Göttingen, Germany.*
**Corresponding authors: Krishnayan Basuroy and Simone Techert.*
*Email ID for correspondance:Krishnayan.basuroy@desy.de*

## ABSTRACT

Pyrene based molecules are inclined to form excimers through self-association upon photoexcitation. In this work, the pyrene core is functionalized with *N*-methylacetamide group at the position 1 or 2, to develop pyren-1-methylacetamide (PyMA1) and pyren-2-methylacetamide (PyMA2), respectively. Upon photoexcitation with 345nm, a portion of molecules in PyMA1 and PyMA2 solutions, at ≥ 1.0mM, have formed static excimers. The steady state spectroscopic measurements suggest that, whether it is the dimerization of molecules in ground state (GS) or in excimer formation, characteristic signs are more pronounced in PyMA1 than its isomeric counterpart, PyMA2. The shift of the excimer band in their respective emission spectra suggest that the extent of overlap in π-π stacking is greater for PyMA1 than PyMA2, in the excited state. The optimized geometry of dimers in toluene shows that overlapping area between the pyrene moieties in π-π stacking between the dimers is greater for PyMA1 than PyMA2, in GS. The natural bond orbital (NBO) analysis with the optimized GS geometries show that stabilization/interaction energy between the dimers in π-π stacking is higher in PyMA1 compared to PyMA2, in toluene. The transient absorption (TA) measurements, in toluene, over fs-ps regime (fs-TA) showed that the formation of static excimers with pre-associated dimers, in PyMA1, happens in ~700*fs*, whereas, the excimers for the pre-associated dimers in PyMA2 have formed in slightly slower time scale (~1.95*ps*). Contrary to what was observed in solution, the extent of overlap in π-π stacking is lower for PyMA1 dimers (~17%) than PyMA2 dimers (~37%), in single crystals.

## I. INTRODUCTION

Pyrene based fluorophores have attracted an appreciable amount of interest, owing to their long-lived singlet excited state,[1] high fluorescence quantum yield,[2] good thermal stability[3] and high charge carrier mobility[4,5]. These features make pyrene based systems suitable for designing a wide range of organic electronic devices, such as organic light-emitting diodes (OLEDs), organic photovoltaics (OPVs), organic field-effect transistors (OFETs) and organic lasers.[5] However, a major shortcoming of using pyrene based luminescent materials is the extreme sensitivity of their fluorescent property towards fast non-radiative quenching of the monomeric fluorescence at close aggregation, a phenomenon, known as aggregation caused quenching (ACQ).[6] In pyrene based systems, the ACQ of monomeric fluorescence is often accompanied by aggregation-induced excited state dimers, known as excimers.[7-9] Excimer formation drastically quenches the monomeric emission in the aggregation state and can function as trap states that restrict the targeted processes such as energy transfer and exciton diffusion, making it undesirable for energy conversion or light-harvesting applications.[10-13] On the other hand, recent evidences have shown that excimer formation has facilitated the singlet fission process.[14-16] The excimer-induced enhanced emission (EIEE) in pyrene based systems also shows that the excimers possess higher photoluminescence efficiency compared to their monomeric counterparts.[17,18] White light emitting (WLE) materials are also designed by exploiting the easy tunability of the well separated monomer and excimer emission bands across the entire visible wavelength range.[19,20] Pyrene based excimers are also utilized as fluorescent probes to detect the presence of transition metals and examine protein-protein interactions.[21-23]

Depending on how they form, excimers can be divided into two classes, static and dynamic.[24] The static excimers are formed due to the photoexcitation of ground state dimers that are already pre-associated through π-π stacking or van der Waals interactions. The dynamic excimers are formed due to interaction between the molecules in the lowest-lying singlet excited state with identical molecules in the ground state. Recently, a $C_3$-symmetric molecular probe (PYTG) consisting of pyrene and triaminoguanidinium chloride has been utilized to understand the static and dynamic excimer formation in a single molecule platform, where the dynamic excimer was formed by changing the concentration and the static excimer was formed in the presence of specific ions.[25]

In this manuscript, we have investigated two mono-substituted, isomeric pyrene derivatives, pyren-1-methylacetamide (PyMA1) and pyren-2-methylacetamide (PyMA2), where pyrene is functionalized by N-methylacetamide group at 1- and 2- positions, respectively. As a conscious effort to utilize the intermolecular hydrogen bond interactions during close

aggregation, we have employed methylacetamide to attach to the pyrene ring which contains both hydrogen bond donor (NH) and acceptor (CO) groups. This intermolecular hydrogen bond is expected to facilitate greater overlap of pyrene moieties between the dimers, necessary for the formation of strong excimers.[26] In the present study, a portion of molecules in both the systems form static excimers at 1.0mM, in solution, while exciting with 345nm radiation (SCHEME 1). The dynamics of pyrene excimers, either in gases, solutions or solids, is an ultrafast process, typically occurs in the picosecond or sub-picosecond time scale and makes it technically challenging to study them in real-time situation, even while equipped with ultrafast laser sources and detectors with fast readouts.[27-29] We have employed ultrafast optical transient absorption spectroscopy technique in femtosecond-picosecond (fs-ps) and nanosecond-microsecond (ns-μs) regimes to examine the ultrafast dynamics of transient species followed by the laser excitation.

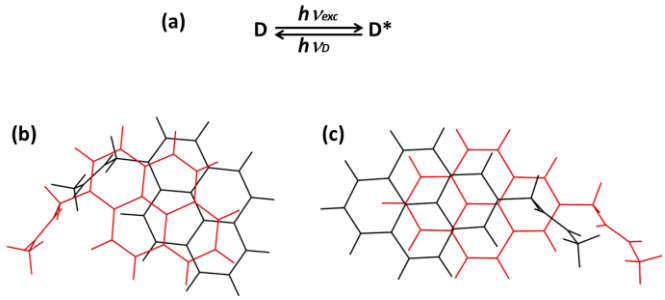


**SCHEME 1.** (a) Kinetic schemes of static excimer formation in PyMA1 and PyMA2 (D = Ground state dimers, D*= excimers). (b) PyMA1 dimer. (c) PyMA2 dimer.

## II. EXPERIMENTAL SECTION

### A. Synthesis and Steady-State Spectroscopy

PyMA1 and PyMA2 (Fig. 1a,b) were synthesized adopting the procedures mentioned in the literature.[30-33] UV-Vis absorption spectra were collected using a Cary-5E UV-VIS spectrophotometer (Varian Australia).[34] The wavelength interval was 0.5nm and the path length of the beam inside the cuvettes were 1mm and 10mm. The absorption spectra for the compound of interest were corrected using a reference spectrum corresponding to the solvent that is used to dissolve the compound. All the measurements were carried out at RT.

Jobin Yvon Horiba Model Fluorolog 3 FL3 22 equipped with, both, front-face (22°) and right angle (90°) detection was used to collect the fluorescence emission and excitation spectra. The instrument is also equipped with 450 W Xenon lamp for excitation. The measurements were performed using 3mm and 10mm path length quartz cuvettes. All the spectra were corrected using the correction files available in the Horiba software that deals with the excitation light intensity and photomultiplier (PMT) response. While collecting the fluorescence emission spectra the width of the entrance and exit slit width was 2nm for both emission and excitation. In case of collecting fluorescence excitation spectra, for PyMA1, the entrance and exit slit width for excitation was 2nm and for emission it was 1nm. While for PyMA2, the entrance and exit slit width for excitation was 3nm and for emission it was 1nm. The measurements in the solutions were performed after purging with $N_2$ gas for 15-20 minutes. We have also used Agilent Cary Eclipse Fluorescence Spectrophotometer to measure some of the spectra.

Apart from the 0.1mM and 1.0mM, we have also collected UV-Vis absorption, fluorescence emission and fluorescence excitation spectra at other concentrations. We have also collected the emission spectra for both the systems with methanol in order check the effect of a polar solvent on the excimer bands.

### B. X-ray Diffraction

Suitable single crystals of PyMA1 and PyMA2 were grown in ethyl acetate/ethanol mixture by slow evaporation. X-ray data at 80K were collected on undulator synchrotron radiation with λ = 0.62073 Å at P11 beamline in PETRA III, DESY, Hamburg, Germany. Crystal data and structure refinement parameters are provided in Table S1. Indexing of the X-ray diffraction pattern, unit cell refinement and spot integration were performed with XDS.[35] The crystal structures were solved and subsequently refined using the X-ray diffraction datasets collected at 80K for both the compounds. All the X-ray diffraction data sets were collected in phi scan type mode. For both the compounds, the crystal structure was solved using direct methods in SHELXS.[36] All the structures were refined against $F^2$ isotropically, followed by full matrix anisotropic least-squares refinement using SHELXL-97.[37] For both the structures, all the hydrogen atoms were fixed

geometrically, in idealized positions, and allowed to ride with the respective C or N atoms to which each was bonded, in the final cycles of refinement. CCDC deposition numbers for the compounds are 1896002 (PyMA1) and 1896013 (PyMA2) which contain the supplementary crystallographic data for this paper and can be obtained free of charge from The Cambridge Crystallographic Data Centre via www.ccdc.cam.ac.uk/data_request/cif.

### C. Time-correlated single photon counting

Photoluminescence (PL) spectra and lifetimes were measured at the Center for Nanoscale Materials (CNM) at Argonne National Laboratory, using a home-made fluorescence microscope fitted with a liquid nitrogen cooled continuous flow cryostat (Janis ST-500UC) in CNM. The instrument was based on an Olympus IX-71 inverted microscope. A pulsed 375nm laser (PicoQuant, DC375M) operated at 4MHz was used to excite the sample through a ThorLabs LMU-15X-NUVobjective that was used to both focus the incoming laser light and collect the emitted PL. The collected PL was separated from the exciting laser using a dichroic mirror and a bandpass filter (both Semrock). The PL was then routed either to a spectrograph (Princeton Instruments, SpectraPro-300) fitted with a CCD camera (Princeton Instruments, PIXIS) or, for lifetime measurements, to a fiber-coupled single photon avalanche diode (SPAD) (Micro Photon Devices, PDM). The output from the SPAD and a trigger pulse from the laser power supply were fed to the two input channels of a time-correlated single photon counting (TCSPC) system (PicoQuant, PicoHarp 300).

### D. Quantum Chemical Calculations

All the quantum chemical gas phase calculations with monomers were performed using DFT methods at B3LYP/6-311G** level of theory using the Becke[38] three-parameter hybrid functional and Lee–Yang–Parr's[39] gradient-corrected correlation functional (B3LYP) implemented in the Gaussian16 (G16)[40] package. GaussSum 3.0 was used to plot the density of states diagram.[41] GaussView 6.0 was used to plot the frontier orbitals.[42]

The geometry optimization and natural bonding orbital (NBO) calculation with dimers in toluene were performed at M06-2X/6-311G** level of theory. The hybrid Minnesota functional M06-2X is considered to be more successful while dealing with dispersion interactions, compared to B3LYP.[43] The solution phase calculation was performed in the presence of toluene by placing the dimers in a cavity within the solvent reaction field. The NBO's were plotted using ChemCraft software.[44] All calculations were initiated with experimentally obtained single crystal geometry from X-ray diffraction measurements. A brief discussion on the method of calculating the percentage of overlap between the π-π stacked pyrene moieties for both the systems, are also provided.

### E. Optical Transient Absorption Spectroscopy

Ultrafast transient absorption (TA) spectra and kinetics were carried out at the Center for Nanoscale Materials (CNM) at Argonne National Laboratory using an amplified Ti:sapphire laser system (Spectra Physics, Spitfire-Pro) and automated data acquisition system (Ultrafast Systems, Helios). The amplifier produced 120fs pulses at 5kHz. The output from the amplifier was split 90/10 to pump an optical parametric amplifier (TOPAS) and to generate a continuum (450-750nm) probe. The TA system enables three-dimensional data collection (spectra/time/ΔOD). The continuum probe beam was generated by first sending the 10% output from the laser amplifier down a computer controlled optical delay line then focusing into a 3mm thick piece of sapphire. The residual 800nm light was removed from the probe beam with an interference filter. The probe beam was then focused using a 20X microscope objective onto a horizontally held 2mm quartz cuvette containing a solution. The transmitted probe beam was detected using a fibre optically coupled spectrograph with a 1D, 2048-pixel CCD array detector. The excitation beam was overlapped on the probe beam spot on the sample at an incident angle of ca. 15 degrees after being optically chopped at 2.5kHz using a synchronous chopper so that the spectrograph measured the transmitted probe beam alternatively as $T_{ON}$ and $T_{OFF}$. The differential extinction $\Delta A = \log_{10}(T_{ON}/T_{OFF})$ was calculated for each pair of pulses and was typically averaged over a two second interval for each delay time. Temporal chirp in the probe pulse was measured and corrected for by making a measurement on neat solvent; the resonant signal was then fitted for each probe wavelength to determine the zero-delay position between pump and probe. For the measurements, typical experimental excitation parameters were: 200μW at 345nm. The probe beam is focussed to typically ~150-200μm spot. It is necessary to make sure that no area is getting probed which is not pumped first. The pump beam size is always slightly bigger than the probe beam since there is some spatial chirp on the probe beam. In both the temporal mode of data collection, HELIOS (0-3ns) and EOS (0-400μs), the pump beam is the same the only difference is the probe beam. The probe is generated differently for both the modes. For HELIOS mode, Sapphire (~440-760) crystal is used and for EOS mode, a fibre coupled continuum laser with ~370-900nm spectrum is used. For fs-ps regime, in the HELIOS mode, the excited state absorption was measured between -1.00ps to 2.84ns. First 1ps with 100fs step size, next 5ps with 50fs step size, next 500ps with 5ps step size and finally 2336ps with 20ps step size. The

smallest step size was kept between 0 to 5ps with 50fs as most of the ultrafast processes were expected to observe in this time interval. In EOS mode the temporal resolution was 100ps throughout the measurement range. The measurements in the solutions were done after purging with $N_2$ gas for 15-20 minutes. All the solutions were continuously stirred with the help of a rotating magnet, while placing a small magnetic stir bar inside the cuvette. The magnet was rotating at 650rpm. TA datasets were processed using Surface Xplorer software provided by Ultrafast Systems.

## III. RESULTS AND DISCUSSION

### A. Steady-State Spectroscopy

A comparative analysis of the UV-Vis absorption, fluorescence emission spectra and excitation spectra collected for PyMA1 and PyMA2, in toluene, at 0.1mM and 1.0mM concentrations, was performed. At 0.1mM, both PyMA1 and PyMA2 have exhibited mostly monomeric characteristics, with no sign of close aggregation (Fig. 1c,d). However, the UV-Vis absorption spectra for both, PyMA1 and PyMA2 show that the ratio of the first two vibronic peak intensities, i.e., 0–0/0–1 corresponding $S_2 \leftarrow S_0$ transition, decreases with increasing concentration (Fig. 1c,d). This particular sort of change in relative vibronic peak intensities with concentration indicates the formation of H-aggregates, i.e., pre-association of electronically interacting molecules in the ground state, with positive, "H-type", excitonic coupling.[45,46] These changes are much more prominent for PyMA1, indicating higher extent of aggregation compared to the isomeric counterpart, PyMA2. According to Laporte rule, due to the centrosymmetric nature of pyrene moiety, $S_1 \leftarrow S_0$ vertical transition remains symmetry-forbidden for both the systems. Nonetheless, due to substitution of N-methylacetamide on pyrene ring, the symmetry of the pyrene ring has been affected and a very weak $S_1 \leftarrow S_0$ vertical transition, at ~375nm was observed, on the absorption spectra for both the systems. The fluorescence spectroscopy with 345nm excitation reveals the excimer formation for both the compounds at 1.0mM, with the appearance of bathochromically shifted, broad and structure-less band in the emission spectra. By deconvoluting the emission spectra, it was evident that the excimer bands corresponding to PyMA1, centred at ~475nm, are bathochromically shifted from the excimer band observed for PyMA2, centred at ~448nm (Fig. S1). If we correlate this phenomena to what was observed elsewhere, for the crystals of pyrene derivatives, it can be argued that the dimers formed by π-π stacking in PyMA1 has greater overlap between the π systems compared to PyMA2, in toluene at 1.0mM, which is reflected in the redder shifted excimer emission.[47] In comparison to what was observed at 0.1mM, the overall emission intensity from both the systems at 1.0mM are reduced by ~2.5 fold and ~8 fold for PyMA1 and PyMA2, respectively (Fig. S2). The relative intensity of excimer bands compared to monomer bands in emission spectra also suggested that excimer formation is much more pronounced in PyMA1 than PyMA2. Which again, could be resulted due to the fact that either the strength of excitonic coupling or the population of dimers, or a culmination of both are greater in PyMA1 than PyMA2, at 1.0mM, in solutions. Contrary to what is observed/inferred from the emission spectra in solution, the single crystal structures obtained from X-ray diffraction measurements suggest that in single crystals, the overlapping area between the **π-π** stacked pyrene moieties in PyMA1 dimers are lower than PyMA2 dimers.

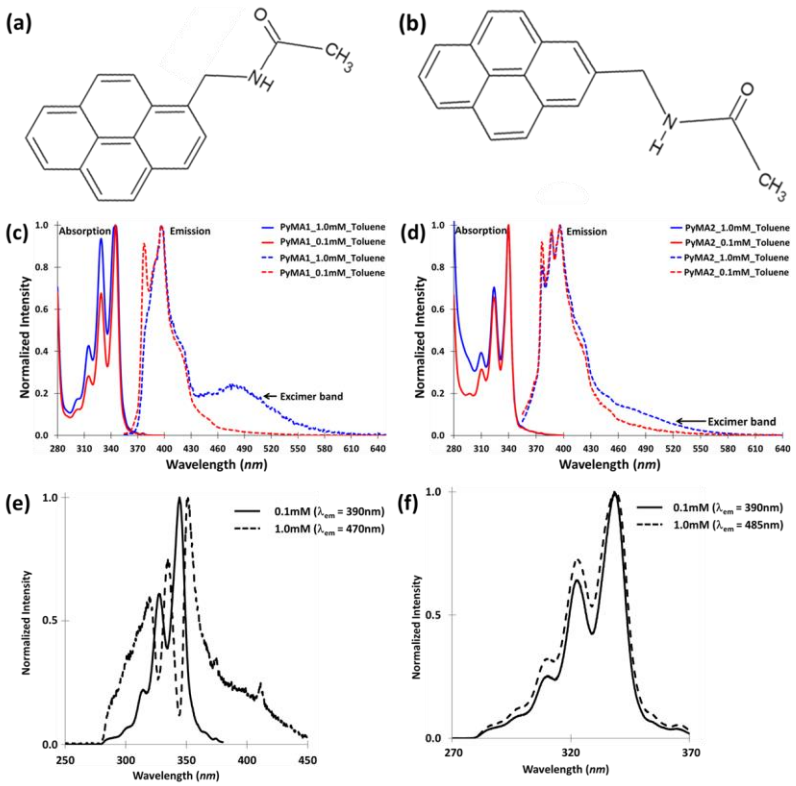


**FIG. 1.** Chemical structure of (a) PyMA1 and (b) PyMA2. Normalized absorption (solid lines) and emission spectra (dashed lines) of (c) PyMA1 and (d) PyMA2 at 0.1mM (red) and 1.0mM (blue). $\lambda_{exc}$ = 345nm. Solvent = Toluene. Normalized excitation spectra of, (e) PyMA1 and (f) PyMA2, at 0.1mM (solid lines) and 1.0mM (dashed lines) (with 10mm cuvette).

The fluorescent excitation spectra of PyMA1 show not only a drastic change in the shape of the spectrum but also a significant bathochromic shift along with the changes in the relative intensity of the low energy excitation bands, while increasing concentration from 0.1mM to 1.0mM (Fig. 1e). For PyMA2, there is no shifting of the excitation bands from 0.1mM to 1.0mM. However, small changes in relative intensity of the low energy bands along with very little broadening, were observed in the excitation spectrum of PyMA2 (Fig. 1f). Also, in the excitation spectra of PyMA2, for 0 – 0 transition, the peak-to-valley intensity ratio at 0.1mM, $P_{0.1mM}$ (~2.4), is larger than the peak-to-valley intensity ratio at 1.0mM, $P_{1.0mM}$ (~1.9), suggesting pre-association in the ground state.[24] Moreover, it is quite possible that these two isomeric pyrene derivatives, with a very similar effective hydrodynamic radius as well as a very similar mode of intermolecular interactions, would have either very similar diffusion coefficient in a solvent/solution or very similar mode/amplitude of orientational changes in a confined environment, at a given concentration.[48] Therefore, the substantial differences observed in the fluorescence excitation spectra between PyMA1 and PyMA2 at 1.0mM, cannot be entirely attributed to their differences in the extent of aggregation. A difference in the overlapping area of π-π stacking between the pyrene moieties as well as the interplanar distance between them may have created a difference in the excitonic coupling strength between the dimers in these systems. Since the excitation spectrum of PyMA2 does not show a spectral shift at 1.0mM, the dimeric excitonic coupling can be considered weaker in PyMA2 than PyMA1.[49] Although, a more precise way that one can calculate the excitonic coupling strength between the dimers is by comparing the simulated absorption spectra with the measured absorption spectra.[50]

While the absorption spectra suggested a greater extent of aggregation for PyMA1 compared to PyMA2, the excitation and emission spectra for PyMA1 may have indicated a stronger excitonic coupling and a greater extent of overlap between pyrene moieties in π-π stacking between the dimers, respectively, compared to its isomeric counterpart, PyMA2, at 1.0mM. Which suggest that the greater extent of overlap in π-π stacking, responsible for excimer formation, may have caused the higher excitonic coupling.

Later, a series of steady-state absorption, emission and excitation spectra were collected for PyMA1 and PyMA2 in toluene and methanol at an array of concentrations (Fig. S2–S6). The fluorescence emission spectrum for PyMA2 collected in toluene shows that while the excimer band is not very pronounced even at 4.0mM concentration (Fig. S6a), the excitation spectra at a concentration ≥ 1.0mM shows a clear sign of pre-association in the ground state (Fig. S4b).

### B. Quantum Chemical Calculations

***Dimers***

Quantum chemical calculations with DFT methods were employed to anticipate the electronic transition energies and intensities of singlet to singlet transitions for the monomers. The detailed discussion on monomeric calculations are provided in the supporting information. In order to have a better understanding of the pre-association/dimerization in the ground state for PyMA1 and PyMA2, geometry optimization of the dimers at M06-2X/6-311G** level of theory was performed. As reported elsewhere, the hybrid Minnesota functional, M06-2X which includes long-range dispersion correction, proved to be quite successful in describing dispersion interactions in the neutral molecules studied here.[43,55] The optimized geometries obtained from gas phase and solution phase (toluene) DFT calculations suggest that the dimers in PyMA1 have higher extent of overlap (~47% in gas and ~50% in toluene) (Fig. 2a,b) in π-π stacking between the pyrene moieties, compared to PyMA2 (~43% in both gas phase and toluene) in ground state (GS) (Fig. 2c,d). The theoretically obtained results are in good agreement with what is inferred from the emission spectra in solutions. As we have mentioned earlier, the above-mentioned observation regarding the extent of overlap is quite different to what is observed for PyMA1 and PyMA2 in single crystal structures. A brief description of the method of calculating the overlap between π-π stacked pyrene moieties are provided in the supporting information. Single point (SP) energy calculation with optimized geometry was performed with the aid of counterpoise method to correct the basis-set superposition error (BSSE).[56] The SP energy values of different geometries along with the complexation energy of the dimers, obtained from the counterpoise corrections are listed in Tables S8 and S9. The scans of potential energy surface (PES) at M06-2X/6-311G** level of theory with redundant internal coordinates, in gas phase, using the intermolecular hydrogen bond (H···A) distance between the dimers suggest that the dimers are energetically more stable in PyMA1, compared PyMA2 at a distance ranging from 1.6 to 2.5 Å (Fig. 2e).

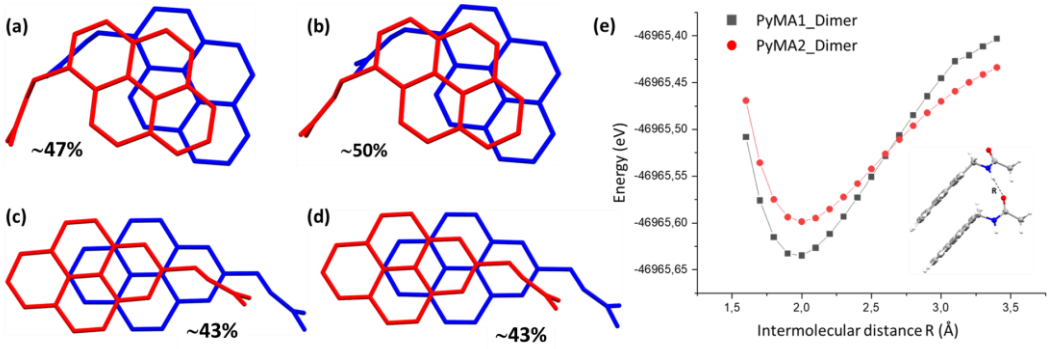


**FIG. 2.** Overlap of pyrene moieties in π-π stacking of dimers, obtained from optimized geometry provided by quantum chemical calculations. Dimer geometry optimized, in gas phase (a) PyMA1, (c) PyMA2 and in solution phase (toluene) (b) PyMA1 (d) PyMA2. Percentage of overlap area is indicated on the figures. (e) The potential energy surface (PES) for PyMA1 and PyMA2 dimers obtained by scanning the intermolecular distance *R*.

To calculate the interaction energies between the dimers in the optimized GS geometries, we have performed natural bond orbital (NBO)[57] analysis at M06-2X/6-311G** level of theory in solution phase (toluene). The NBO analysis allowed us to estimate the donor-acceptor interaction energies between the dimers, from 2nd order perturbation theory analysis of Fock matrix in NBO basis.[57] The interaction energies provide a measure of the strength of non-covalent interactions between the dimers. The intermolecular interaction/stabilization energies in dimers, involving the π-π stacking of pyrene moieties and N-H…O=C interactions with E(2) ≥ 0.05kcal/mol, for both the systems, are listed in Table S10. The NBO analysis in toluene suggest that the intermolecular hydrogen bond is stronger in PyMA2 compared to PyMA1 in GS (Table 1). Whereas, the stabilization energies of π-π stacking involving only the pyrene moieties from dimers are much higher in PyMA1 than PyMA2 (Table 1). Some of the strongest intermolecular interactions, in π-π stacking of dimers, with the donor and acceptor NBO's, for both the systems, in GS, are depicted in Fig. 3 and listed in Table 2. The higher degree of overlap between pyrene moieties in dimers for PyMA1 compared to PyMA2, in optimized GS geometries and subsequently the exhibition of considerably higher stabilization/interaction energy between the dimers regarding π-π stacking in PyMA1 compared to PyMA2 from NBO calculations, suggest that the π-π stacking responsible for the formation of excimers in solution at 1.0mM may have been stronger in PyMA1 than PyMA2.

**Table 1** Stabilization/interaction energy between the dimers for π-π stacking, in PyMA1 and PyMA2, obtained from NBO calculations with optimized geometries in toluene.

| Optimized Geometries in toluene | Overlap % in π-π stacking (%) | Stabilization energy in N-H…O=C interactions (kcal/mol) | Stabilization energy in π-π stacking (kcal/mol) |
|---|---|---|---|
| PyMA1 | ~50 | 9.44 | 20.49 |

| | | | |
|---|---|---|---|
| PyMA2 | ~43 | 11.30 | 18.66 |

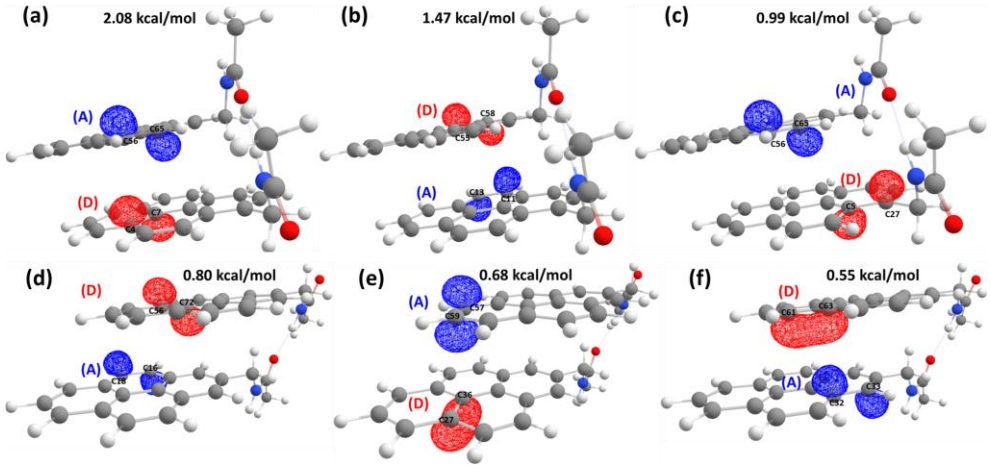


**FIG. 3.** Donor (red) and acceptor (blue) NBO's for the strongest intermolecular interactions between the π-π stacked pyrene moieties of dimers with optimized geometries in toluene are depicted, PyMA1 (a, b, c); PyMA2 (d, e, f). Strength of the interactions are also provided on the diagram.

**Table 2**. Some of the strongest intermolecular interactions between the dimers for π-π stacking, in PyMA1 and PyMA2, based on the 2nd order perturbation theory analysis of Fock matrix in NBO basis, are listed.

| Donor NBO's ($i$) | Acceptor NBO's ($j$) | E(2) (kcal/mol) | E($j$) – E($i$) (a.u.) | F($i$, $j$) (a.u.) |
|---|---|---|---|---|
| PyMA1 | | | | |
| BD*(2) C4-C7 | BD*(2) C56-C65 | 2.08 | 0.02 | 0.01 |
| BD*(2) C55-C58 | BD*(2) C11-C13 | 1.47 | 0.03 | 0.01 |
| BD*(2) C5-C27 | BD*(2) C56-C65 | 0.99 | 0.02 | 0.01 |
| PyMA2 | | | | |
| BD*(2) C56-C72 | BD*(2) C16-C18 | 0.80 | 0.01 | 0.01 |
| BD (2) C27-C36 | BD*(2) C57-C59 | 0.68 | 0.35 | 0.01 |
| BD (2) C61-C63 | BD*(2) C32-C33 | 0.55 | 0.34 | 0.01 |

[Note: E($i$) corresponds to Lewis type "filled" donor orbitals. E($j$) corresponds to non-Lewis type "unfilled" acceptor orbitals. BD = 2-center bond, BD* = 2-center anti-bonds.

For each donor NBO ($i$) and acceptor NBO ($j$), the stabilization energy $E(2)$ associated with $i \rightarrow j$ delocalization is determined as,

$$E(2) = \Delta E_{ij}^{(2)} = \frac{q_i F(i,j)^2}{\varepsilon_j - \varepsilon_i}$$

Where, $q_i$: is the donor orbital occupancy.

$\varepsilon_i$, $\varepsilon_j$ are diagonal elements (orbital energies) of NBO Fock matrix.

$F(i,j)$ is the off-diagonal NBO Fock matrix elements.]

### C. Single Crystal X-ray Diffraction

Single crystal structures of PyMA1 and PyMA2 shed light on the intermolecular interactions between the dimers and the extent of the overlapping of the pyrene moieties, in solid state. The molecular conformations of PyMA1 and PyMA2 in single crystals at 80K are quite similar (Table S2 and S3). In both the crystal structures, N-H···O hydrogen bond and π···π interactions between the unit translated molecules are holding the entire packing of molecules and the distance and angle parameters suggest that the extent of the interactions are very similar in both the crystals (Fig. 2a,b; Fig. S7, S8, S9 and S10; Table S4 and S5). Contrary to what was inferred from the emission spectra in toluene, the extent of overlap between the π-π stacked pyrene moieties in PyMA2 dimers (~37%) are greater than PyMA1 dimers (~17%) in single crystals as the X-ray diffraction study at 80K suggests (Fig. 2c,d).

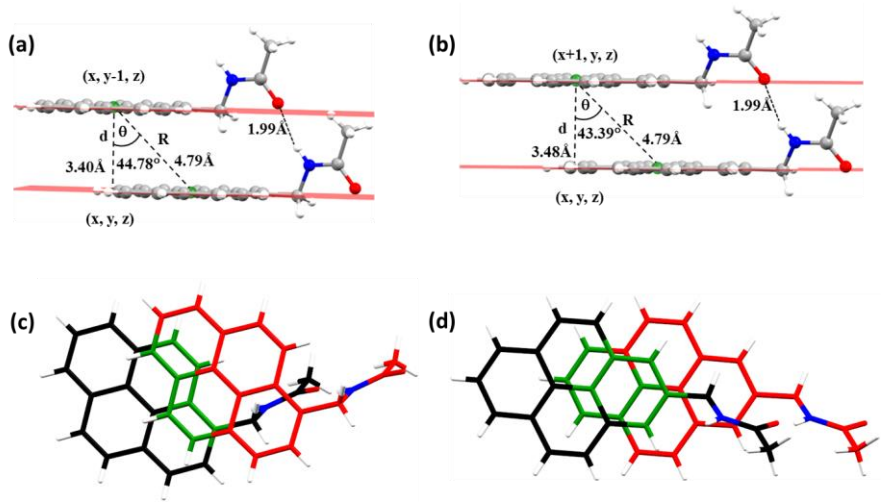


**FIG. 4.** The parallel displaced π···π interactions and intermolecular N-H···O hydrogen bond interaction between the unit translated molecules in (a) PyMA1 and (b) PyMA2. Centroids are shown in green. Extent of overlap between the pyrene rings of unit translated molecules, (c) PyMA1 (~17%) and (d) PyMA2 (~37%) are showed with green colored atoms. The carbon atoms of the unit translated molecules are colored in red and black. Krishnayan Basuroy, Jose de J. Velazquez-Garcia, Darina Storozhuk, David J. Gosztola, Sreevidya Thekku Veedua and Simone Techert, arXiv:2103.03002v1 [cond-mat.mtrl-sci], 2021; licensed under a Creative Commons Attribution (CC BY) license.

### D. Time-Correlated Single Photon Counting (TCSPC)

The time-correlated single photon counting (TCSPC) technique was employed to determine the decay lifetime of the emissive species for both PyMA1 and PyMA2 in solution and single crystals (Table S6; Fig. S11). A pulsed 375nm laser operated at 4MHz was used to excite all the samples. In toluene, emissive species in PyMA1 and PyMA2 decay mono-exponentially with decay lifetimes in the range of ~1-3*ns* through all concentrations (Table S6; Fig. S11a). This short lifetime can be attributed to an alternative excited state decay pathway through incorporation of methylacetamide.[51,52] However, at 1.0mM, PyMA1 shows a lifetime of ~29*ns* with a small contribution (~0.02%), which can be identified as excimer emission. The lifetimes measured for both systems at 1.0mM are considerably longer than at 0.1mM (Table S6). In single crystals, both PyMA1 and PyMA2 decay bi-exponentially when excited at 375nm, suggesting the presence of both monomeric and excimer species. As the temperature was slowly reduced from 296K to 77K, the excimer species population gradually increased in PyMA1 and PyMA2 crystals from 1% to 5% and 2% to 11%, respectively (Table S6; Fig. S11b and S11c). The π-π overlap between the pyrene moieties belonging to the unit translated molecules in PyMA2 (~37%) is comparatively better than PyMA1 (~17%) at 80K and must have caused the higher lifetime as well as the percentage of excimers for the former.[47] Although, for PyMA1, the excimer lifetime systematically decreased from ~35.6*ns* to ~23.5*ns* with the gradual reduction of temperature, for PyMA2, the excimer lifetimes do not change much through the different temperatures.

### E. Optical Transient Absorption Spectroscopy

The excited-state absorption of the transient species in PyMA1 and PyMA2 were investigated by ultrafast optical transient absorption (TA) spectroscopy. We have employed ns-TA (EOS mode) and fs-TA (HELIOS mode) to explore the excited state dynamics of the pyrene-N-methylacetamide isomers in the ns-μs and fs-ps time domains, respectively. PyMA1 and PyMA2 solutions at 1.0mM, in toluene, were excited by 345nm laser radiation at 200μW and subsequently probed with a weak white-light continuum probe. The selection of excitation wavelength is crucial to remove ambiguity while studying

the kinetics and mechanism of excimers.[58] During the TA data collection we have depolarized the pump beam by placing a depolarizing optic in the pump (excitation) beam path, avoiding the collection of spectral artefacts in decay kinetics from the rotation of polarizable molecules. Prior to the measurements, the solutions were purged with $N_2$ gas. For HELIOS mode, the continuum probe ranges between ~440-760nm, whereas for EOS mode, a fibre-coupled continuum laser with ~370-900nm spectrum is used as the probe. TDDFT calculations and spectroscopic measurements have suggested that the excitation with 345nm radiation will take PyMA1 and PyMA2 molecules into the excited state singlet $S_2$ from $S_0$ ($S_2 \leftarrow S_0$ transition). Followed by the excitation into $S_2$, the monomers would rapidly go through a fast-internal conversion (IC) process into the $S_1$ state. The absence of any relevant negative signal (ground-state bleach) could be attributed to the spectral range of probing in TA spectra, which is outside the region of ground-state absorption and also to a high molar absorptivity for singlet – singlet ($S_N \leftarrow S_1$) and triplet – triplet ($T_N \leftarrow T_1$) absorption within the same spectral range.

Fig. 5a shows the formation of two major bands in the fs-TA spectrum of PyMA1, centred on ~520nm and ~595nm, almost simultaneously (Inset: Fig. 5a). The evolution of the absorption band around 595nm, in ~560*fs*, can be identified as the formation of monomeric $S_2$ state of PyMA1. A similar sort of band for pyrene monomers is also commonly observed around ~585nm.[59] The decay of 595nm band in ~160*fs* by radiation less internal conversion, $S_1 \leftarrow S_2$ transition (IC) of the monomeric species suggest that the quenching time is in good agreement with the previously published results.[27,59] The evolution of the 520nm band which starts forming in ~560*fs* and starts decaying again only after ~5.16*ps*, can be assigned to the absorptions from monomeric $S_1$ state and static excimers, combined. The static excimer component of the broad absorption band centred on 520nm forms completely in ~700*fs* (Fig. 5b). In the light of the decay of 595nm band and the further strengthening of 520nm band till ~ 1.17*ps*, it is possible to infer that the ~520nm band constitutes an overlap of the absorption contributions from both monomeric $S_1$ and static excimers. The overall formation time for the 520nm band is slower than the time scale proposed previously (~140*fs*) for excimer formation in pyrene crystals.[60] In fact, pyrene excimers have strong absorption bands in the wavelength region between 400nm – 550nm which overlaps with the $S_N \leftarrow S_1$ transitions.[27,29,61-63] It is also important to note, as exhibited in Fig. 5, rapid formation of a band centred on 480nm was also observed for both PyMA1 and PyMA2, and can be identified as characteristic Raman signal from toluene, in the form of "coherent artifacts", which completely decays within a few ps (~4ps) (Fig. S17 and S18). The TA spectrum with toluene shows two prominent absorption bands, centred on 480nm and 580nm (Fig. S17 and S18). The 580nm band for toluene perfectly overlaps with the 580nm absorption band observed on the TA spectrum of PyMA2 (Fig. S18).

The fs-TA spectrum for PyMA2 shows the formation of two very broad absorption bands ~530nm and ~580nm. The 580nm band, which forms in ~630*fs*, gets bathochromically shifted to 600nm within ~1.2*ps*, can be identified as the absorption from the monomeric singlet state, $S_2$ (Fig. 5c). The inception of the decay of the 580nm/600nm band is followed by the appearance of the 530nm band, as the isosbestic point around 540-550nm showed. The 530nm absorption band which completely forms within ~1.95*ps*, could be attributed to the contributions from the absorption of monomeric $S_1$ state (Fig. 5d).[27] The correlation between the decay and rise of 580nm/600nm and 530nm absorption bands, respectively, can be witnessed in their respective kinetic profiles while plotted together (Inset: Fig. 5c). Noticeably, the decay of the $S_2$ state is much slower for PyMA2, which could be attributed to the fact that the toluene signal around 580nm overlaps with the signal from PyMA2 (Inset: Fig. 5c). The appearance of the 530nm absorption band along with the prominent shoulder around ~500nm could be attributed to the overlapping contributions from the absorption of monomeric $S_1$ state and the excimers. The fs-TA spectra show that the shoulder around ~500nm started forming around ~629*fs* and becomes prominent by ~1.95*ps* (Fig. 5d). The 530nm band only starts appearing around ~924*fs*, which also coincides with the decay of 580nm/600nm band (Fig. 5d). The kinetic profile corresponding to either the 500nm or 530nm on the fs-TA spectra shows that both the bands starts truly decaying only after ≤65ps (Fig. S19). The proposition of PyMA1 forming static excimers faster than PyMA2 also somewhere acknowledge the fact that pre-associated dimers in PyMA1 may have stronger excitonic coupling than PyMA2.

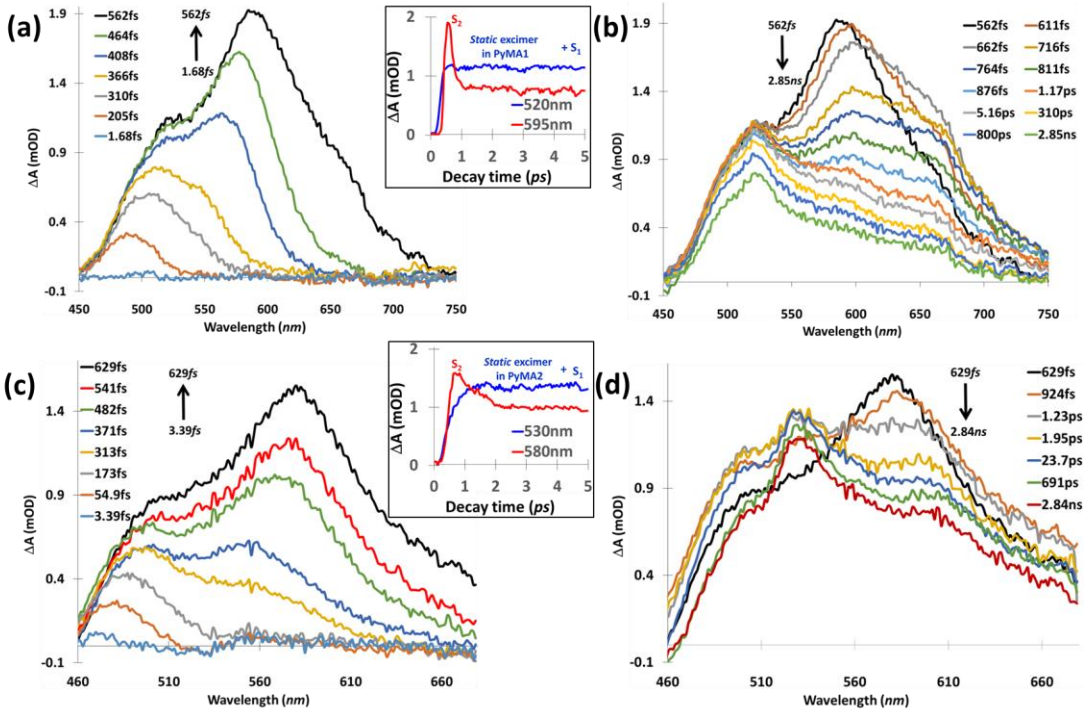


**FIG. 5.** The fs-TA spectra at 1.0mM in toluene. PyMA1 (a, b). PyMA2 (c, d). Inset: Kinetic profile of (a) 520nm and 595nm bands in PyMA1 and (c) 530nm and 580nm bands in PyMA2. ($\lambda_{exc}$ = 345nm). Krishnayan Basuroy, Jose de J. Velazquez-Garcia, Darina Storozhuk, David J. Gosztola, Sreevidya Thekku Veedua and Simone Techert, arXiv:2103.03002v1 [cond-mat.mtrl-sci], 2021; licensed under a Creative Commons Attribution (CC BY) license.

For the analysis of TA data sets, the singular value decomposition (SVD) technique, involving 3-dimensional ΔA vs. time and wavelength spectroscopic data, was employed. It was followed by global analyses to find the principal components responsible for transient signals observed in fs-TA and ns-TA datasets in the form of decay associated spectra (DAS) and the kinetic profile of the decaying components (Fig. S20). The global analyses of fs-TA data collected with PyMA1 show the principle components represented by three right singular vectors in the DAS (Fig. S20a). The first vector (V1) decays tri-exponentially, with the major species, $\tau_1$ (99.3%), affiliated with the DAS centred on 580nm, identified as $S_1 \leftarrow S_2$ IC. Two other minor species, $\tau_2$ and $\tau_3$ represent two slower processes, which could be $S_0 \leftarrow S_2$ fluorescence[64-66] or $T_2 \leftarrow S_2$ ISC[52] (Table S13). Whereas the second component (V2) centred on 520nm and the third component (V3) containing bands centred on 520nm, 600nm and 660nm have decayed only partially (Table S13; Fig. S20a).

The global analyses suggest that the entire fs-TA spectrum for PyMA2 can be associated with three singular vector components, centred on 580nm (V1), 530nm (V2) and 485nm (V3) (Fig. S20b). The decay profile of the right singular vector V1 from SVD analysis shows that 93.6% of the molecules in the S2 state depopulate to the S1 state through IC. While the rest of the population decays through slower processes like $S_0 \leftarrow S_2$ transition or $T_2 \leftarrow S_2$ ISC. The other two components centred on 530nm (V2) and 485nm (V3) have decayed only partially (Fig. S20b).

The EOS temporal mode was employed to capture the excited state dynamics in the ns-μs regime with a 100ps time resolution. The ns-TA data sets for PyMA1 and PyMA2 at 1.0mM were collected from 12*ns* till 2$\mu$*s*. The ns-TA spectra of PyMA1 and PyMA2 are quite similar (Fig. 6). In the beginning, the spectrum for PyMA1 shows a broad band centred on 490nm, with a prominent shoulder at 520nm, which starts decaying after ~12.6*ns* and the 520nm shoulder takes the shape of a distinct band, well separated from the 490nm band. The relative intensity of the 520nm band had also increased with respect to the 490nm band, with time (Fig. 6a). Whereas, for PyMA2, the 490nm and 530nm absorption bands were well separated from the beginning and started decaying after ~12.7*ns*. Although, quite similar to PyMA1, the ns-TA spectrum of PyMA2 also indicated that the relative intensity of the 530nm absorption band had increased with respect to the 490nm band, while decaying. The 520nm and 530nm absorption bands, for PyMA1 and PyMA2, respectively, can be identified with the overlapping of absorption contributions originated from monomeric triplet and excimer singlet. For both the systems, the decay of the 490nm band is juxtaposed with the rise of the 425-428nm band which forms in ~40*ns* and ~50*ns* for PyMA1 and PyMA2, respectively. The 490nm and 425-428nm absorption bands could be identified mostly from monomeric singlet and triplet respectively, as suggested by the isosbestic point around 450-460nm region in the ns-

TA spectra as well as in their corresponding kinetic profiles obtained from SVD analysis (Fig. S21). The global analyses of the ns-TA spectrum for PyMA1 suggest the presence of two components or right singular vectors (Fig. S20c). The right singular vector V1 at 480nm has two components; the majority (~75%) decays through $S_0 \leftarrow S_1$ monomeric transition, while the second component (~25%) that decays in ~255*ns* can be identified as a monomeric triplet (Table S14). The reduction of triplet lifetime, at least by an order, could be due to the presence of residual oxygen in the solution. The right singular vector V2 has two components centred on 425nm and 525nm. While the component at 425nm decays mono-exponentially with a lifetime ~239*ns*, the 525nm component decays bi-exponentially with lifetimes ~28*ns* and ~240*ns*. While the longer lifetime in the 525nm band could be identified as the monomeric triplet, the shorter lifetime could be identified as excimer singlet.

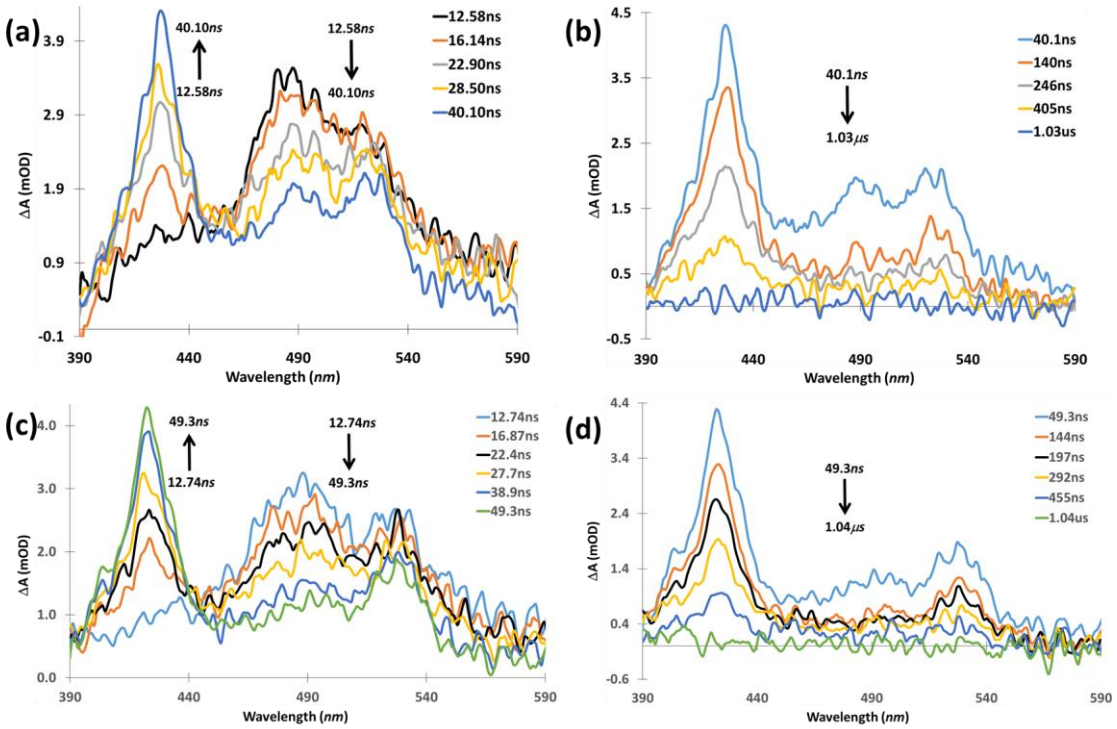


**FIG. 6.** The ns-TA spectra of PyMA1 (a, b) and PyMA2 (c, d) at 1.0mM, in toluene. ($\lambda_{exc}$ = 345nm). Krishnayan Basuroy, Jose de J. Velazquez-Garcia, Darina Storozhuk, David J. Gosztola, Sreevidya Thekku Veedua and Simone Techert, arXiv:2103.03002v1 [cond-mat.mtrl-sci], 2021; licensed under a Creative Commons Attribution (CC BY) license.

For PyMA2 also the global analyses of the ns-TA data suggest two right singular vectors that represent all the transient absorption signals (Fig. S20d). The right singular vector V1 at 480nm decays bi-exponentially with 78% decaying through $S_0 \leftarrow S_1$ monomeric transition, and the rest of the 22% that decays in ~263*ns* can be identified as monomeric triplets. As observed for PyMA1, the right singular vector V2 at 425nm for PyMA2 represents monomeric triplets with a lifetime of ~258*ns*. The decay of the right singular vector V2 at 530nm for PyMA2 exactly resembles the decay of the right singular vector V2 at 525nm for PyMA1. The right singular vector V2 at 530nm in PyMA2 decays bi-exponentially in ~21*ns* (~28%) and ~253*ns* (~72%), indicating similar population percentages of the decaying species in solution, quite like PyMA1 (Table S14). This also suggests that in the context of ground state dimerization, as predicted earlier, extent of aggregation was not the only crucial factor for the differences observed between the steady-state spectra, collected for PyMA1 and PyMA2. The excitonic coupling strength must have also played a significant role, since the ns-TA spectroscopic study suggested quite a similar population percentage for the excimers for both the systems.

## IV. CONCLUSIONS

Pyrene based systems are mostly used in studies which are focused on investigation of electron and proton transfer properties in electron donor-acceptor systems.[4,67] Due to its planar structure, pyrene is already known to be susceptible to

π-π stacking, essential for excimer formation. In fact, the need of functionalizing pyrene comes from the idea of getting rid of the excimer formation by π-π stacking. Therefore, excimer formation in intermolecular hydrogen bonded dimers is not studied much in the context of pyrene derivatives. Our study highlights the tuning of optical properties through vibronic coupling in concentrated pyrene-based systems by small structural modifications, a field that can be explored in the context of novel OLEDs, based on dyes in aggregated states. Therefore, a serendipitous encounter of static excimers for two isomeric mono-substituted pyrene derivatives, with the possibility of varied extent of excitonic coupling, where N-methylacetamide is substituted on pyrene at two different positions, is highly encouraging. This also inspires to explore the possibility of designing different excimer types in pyrene-based systems.

The excitation wavelength of 345nm proved to be crucial for observing the characteristic details of the excimer formation in this case. While exciting the systems with 375nm, the formation of excimers is not so evident in solutions but quite noticeable in the single crystals. It could be that in solution, it was not possible to excite the 375nm band of the pre-associated dimers as at this excitation wavelength they are a minority component compared to the monomers. The intermolecular hydrogen bonds may have contributed to the absence of multiple clusters of molecules with different degrees of overlap in the same solution during dimerization, which reflected in the singular decay time of excimers for both the systems.[59]

The optimized geometries obtained from theoretical calculations in gas phase and toluene suggests that the degree of overlap between the pyrene moieties in π-π stacking is higher in PyMA1 than PyMA2 in ground state (GS). The NBO calculation, in toluene, which provided a quantitative estimation of the strength of interaction energies between the dimers in GS suggested that π-π stacking interactions are stronger in PyMA1 dimers compared to PyMA2. The fluorescence excitation spectra suggest that not only dimerization in GS is more pronounced but the excitonic coupling also may have been stronger in PyMA1 compared to PyMA2. While the theoretical DFT calculations suggested a greater overlap of pyrene moieties in GS for PyMA1 dimers compared to PyMA2 dimers, the emission spectra concluded the same for the excited state (ES) through the observation of the bathochromic shift of excimer band on the emission spectra for PyMA1.

The results obtained from the fs-TA measurements suggest that the pre-associated dimers in the ground state of PyMA1 formed the static excimers much faster (~700*fs*) than the static excimers with pre-associated dimers in PyMA2, which in this case most likely formed within ~1.95*ps*. The reason of additional time for the formation of pre-associated dimers in PyMA2 is not quite clear. Perhaps a stronger π-π stacking in PyMA1 compared to PyMA2 in ground state may have facilitated a faster excimer formation with greater excitonic coupling. It is also observed that the static excimers in both the systems may have a different formation time but their respective lifetimes with ~28*ns* and ~21*ns*, respectively, as shown by ns-TA, are not so different. The excimer lifetimes obtained from the TCSPC study with single crystals closely matches with the results obtained from TA measurements performed in solutions.

Contrary to what was observed in solutions, in single crystals, PyMA2 has better overlap area of π-π stacking between the pyrene moieties (~37%) compare to PyMA1 (~17%). The role reversal of the dimers regarding their overlapping area in π-π stacking, between the solution and solid phase, is quite interesting and therefore warrant a future study that would employ time-resolved photocrystallography measurements to capture the excimer geometry in single crystals.[68-71] Although, in solution the overall emission is quenched for both the systems by varying degree, in close aggregation, several examples of excimer induced enhanced emission (EIEE) are reported recently, which encourages excimer formations to be well utilized in designing multifunctional optoelectronic materials.[72-74] In that regard, pyrene-based systems are better suited than other conjugated systems due to its range and easy tunability of their photophysical properties by substituting different functional groups at different positions. Further studies in the quest to have a better understanding of the ultrafast processes like excimer dynamics are highly desired to design novel multifunctional materials with pyrene-based systems.

## SUPPLEMENTARY MATERIAL

See the supplementary material for Crystal data and structure refinement parameters, conformational analysis of the molecular structures, intermolecular hydrogen bond parameters, packing of molecules in single crystals, steady-state spectra in toluene and methanol, TCSPC results in solution and single crystals, method of calculating the overlap percentage in π-π stacked pyrene moieties, results of theoretical calculations by DFT methods and transient absorption kinetic fit results in toluene.

## ACKNOWLEDGEMENTS

S.T. is grateful for financial support within the ECRAPS and FISCOV Innovation Funds of the Helmholtz Association (HGF). The CMWS-Early Science Program of DESY / HGF is also acknowledged (K.B. and S.T.). Use of the Center for Nanoscale Materials, an Office of Science user facility, was supported by the U.S. Department of Energy, Office of Science, Office of Basic Energy Sciences, under Contract No. DE-AC02-06CH11357. A part of the research was carried out at the light source PETRA-III at DESY, a member of HGF. We would like to thank P11 staff for assistance. K.B. is grateful to Mr. Marten Rittner from Institute for Nanostructure and Solid-State Physics for helping with the measurement of fluorescence emission spectra. J.G.V., D.S., S.V.T. and S.T. acknowledge project B06 of the SFB1073 of the Deutsche Forschungsgemeinschaft (DFG, German Research Foundation) - 217133147/SFB 1073. K.B. acknowledges Dr. Sanjoy K. Mahatha for proof reading and technical feedback in preparing figures. K.B. acknowledges Dr. Sumit Naskar for the discussions on NBO analysis with DFT methods.
We hereby acknowledge that the synthesis has been performed to the largest amount at FS-SCS / DESY, and to small amounts at the Facility for Synthetic Chemistry at the Max-Planck Institute for Biophysical Chemistry.

## Conflicts of interest

There are no conflicts to declare.

## DATA AVAILABILITY

The data that support the findings of this study are available in its supplementary material. Additional data are available from the corresponding author upon reasonable request.

## REFERENCES

1 A. Nakajima, Bull. Chem. Soc. Jpn. **46**, 2602 (1973).
2 H. Maeda, T. Maeda, K. Mizuno, K. Fujimoto, H. Shimizu, and M. Inouye, Chem. Eur. J. **12**, 824 (2006).
3 H. Ran, Z. Zhao, X. Duan, F. Xie, R. Han, H. Sun, and J.-Y. Hu, J. Mater. Chem. C **9**, 260 (2021).
4 S. Techert, A. Wiessner, S. Schmatz, and H. Staerk, J. Phys. Chem. B **105**, 7579 (2001).
5 T. M. Figueira-Duarte, and K. Müllen, Chem. Rev. **111**, 7260 (2011).
6 X. Feng, C. Qi, H.-T. Feng, Z. Zhao, H. H. Y. Sung, I. D. Williams, R. T. K. Kwok, J. W. Y. Lam, A. Qin, and B. Z. Tang, Chem. Sci. **9**, 5679 (2018).
7 Th. Förster and K. Z. Kasper, Elektrochem. **69**, 976 (1955).
8 B. Stevens, Nature, 1961, **192**, 725 – 727.
9 J. B. Birks and L. G. Christophorou, Spectrochim. Acta, 1963, **19**, 401 – 410.
10 A. H. Matsui, Pure Appl. Chem., 1995, **67**, 429 − 436.
11 Z. Chen, V. Stepanenko, V. Dehm, P. Prins, L. D. A. Siebbeles, J. Seibt, P. Marquetand, V. Engel, and F. Wuerthner, Chem. - Eur. J. **13**, 436 (2007).
12 Y. Morishima, Y. Tominaga, S. Nomura, M. Kamachi, and T. Okada, J. Phys. Chem. **96**, 1990 (1992).
13 A. Nowak-Król, B. Fimmel, M. Son, D. Kim, and F. Würthner, Faraday Discuss. **185**, 507 (2015).
14 B. J. Walker, A. J. Musser, D. Beljonne, and R. H. Friend, Nat. Chem. **5**, 1019 (2013).
15 C. M. Mauck, P. E. Hartnett, E. A. Margulies, L. Ma, C. E. Miller, G. C. Schatz, T. J. Marks, and M. R. Wasielewski, J. Am. Chem. Soc. **138**, 11749 (2016).
16 C. E. Miller, M. R. Wasielewski, and G. C. Schatz, J. Phys. Chem. C **121**, 10345 (2017).
17 A. S. Abd-El-Aziz, A. A. Abdelghani, B. D. Wagner, and E. M. Abdelrehim, Polym. Chem. **7**, 3277 (2016).
18 X. –Y. Wang, J. Zhang, J. Yin, and S. H. Liu, Chem. Asian J. **14**, 2903 (2019).
19 A. K. Pati, S. J. Gharpure, and A. K. Mishra, J. Phys. Chem. A **120**, 5838 (2016).
20 T. Wang, N. Zhang, Y. Ge, C. Wang, Z. Hang, and Z. Zhang, Macromol. Chem. Phys. **221**, 1900463 (2020).
21 G. Bains, A. B. Patel, and V. Narayanaswami, Molecules, **16**, 7909 (2011).
22 R. Kubotaa and I. Hamachi, Chem. Soc. Rev. **44**, 4454 (2015).
23 S. S. Razi, R. Ali, P. Srivastava, and A. Misra, RSC Adv. **5**, 79538 (2015).
24 F. M. Winnik, Chem. Rev. **93**, 587 (1993).
25 V. Kumar, B. Sk, S. Kundu, and A. Patra, J. Mater. Chem. C **6**, 12086 (2018).
26 Y. Liu, X. Tao, F. Wang, J. Shi, J. Sun, W. Yu, Y. Ren, D. Zou, and M. Jiang, J. Phys. Chem. C **111**, 6544 (2007).
27 P. Foggi, L. Pettini, I. Sànta, R. Righini, and S. Califano, J. Phys. Chem. **99**, 7439 (1995).
28 J. Hoche, H.-C. Schmitt, A. Humeniuk, I. Fischer, R. Mitrić, and M. I. S. Röhr, Phys. Chem. Chem. Phys. **19**, 25002 (2017).
29 R. D. Pensack, R. J. Ashmore, A. L. Paoletta, and G. D. Scholes, J. Phys. Chem. C **122**, 21004 (2018).

30 E. M. Espinoza, J. A. Clark, J. B. Derr, D. Bao, B. Georgieva, F. H. Quina, and V. I. Vullev, ACS Omega **3**, 12857 (2018).
31 R. O. C. Norman, G. A. Thompson, and W. A. Waters, J. Chem. Soc. **12**, 175 (1958).
32 S. Techert, S. Schmatz, A. Wiessner, and H. Staerk, J. Phys. Chem. A **104**, 5700 (2000).
33 A. G. Crawford, Z. Liu, I. A. I. Mkhalid, M. -H. Thibault, N. Schwarz, G. Alcaraz, A. Steffen, J. C. Collings, A. S. Batsanov, J. A. K. Howard, and T. B. Marder, Chem. Eur. J. **18**, 5022 (2012).
34 A. Ramos and S. Techert, Biophys. J. **89**, 1990 (2005).
35 W. Kabsch, J. Appl. Cryst. **26**, 795 (1993).
36 G. M. Sheldrick, SHELXS-97, A Program for Automatic Solution of Crystal Structures, University of Göttingen, Göttingen, 1997.
37 G. M. Sheldrick, SHELXL-97, A Program for Crystal Structure Refinement, University of Göttingen, Göttingen, 1997.
38 A. D. Becke, J. Chem. Phys. **98**, 5648 (1993).
39 C. Lee, W. Yang, and R. G. Parr, Phys. Rev. B **37**, 785 (1988).
40 Gaussian 16, Revision A.03, M. J. Frisch, G. W. Trucks, H. B. Schlegel, G. E. Scuseria, M. A. Robb, J. R. Cheeseman, G. Scalmani, V. Barone, G. A. Petersson, H. Nakatsuji, X. Li, M. Caricato, A. V. Marenich, J. Bloino, B. G. Janesko, R. Gomperts, B. Mennucci, H. P. Hratchian, J. V. Ortiz, A. F. Izmaylov, J. L. Sonnenberg, D. Williams-Young, F. Ding, F. Lipparini, F. Egidi, J. Goings, B. Peng, A. Petrone, T. Henderson, D. Ranasinghe, V. G. Zakrzewski, J. Gao, N. Rega, G. Zheng, W. Liang, M. Hada, M. Ehara, K. Toyota, R. Fukuda, J. Hasegawa, M. Ishida, T. Nakajima, Y. Honda, O. Kitao, H. Nakai, T. Vreven, K. Throssell, J. A. Montgomery Jr., J. E. Peralta, F. Ogliaro, M. J. Bearpark, J. J. Heyd, E. N. Brothers, K. N. Kudin, V. N. Staroverov, T. A. Keith, R. Kobayashi, J. Normand, K. Raghavachari, A. P. Rendell, J. C. Burant, S. S. Iyengar, J. Tomasi, M. Cossi, J. M. Millam, M. Klene, C. Adamo, R. Cammi, J. W. Ochterski, R. L. Martin, K. Morokuma, O. Farkas, J. B. Foresman, and D. J. Fox, Gaussian, Inc., Wallingford CT, 2016.
41 N. M. O'boyle, A. L. Tenderholt, and K. M. Langer, J. Comp. Chem. **29**, 839 (2008).
42 GaussView, Version 6, R. Dennington, T. A. Keith, and J. M. Millam, Semichem Inc., Shawnee Mission, KS, 2016.
43 M. Walker, A. J. A. Harvey, A. Sen, and C. E. H. Dessent, J. Phys. Chem. A **117**, 12590 (2013).
44 G. A. Zhurko Chemcraft - graphical program for visualization of quantum chemistry computations. Ivanovo, Russia, 2005. https://www.chemcraftprog.com.
45 A. T. Haedler, H. Misslitz, C. Buehlmeyer, R. Q. Albuquerque, A. Köhler, and H.-W. Schmidt, ChemPhysChem **14**, 1818 (2013).
46 F. C. Spano, Acc. Chem. Res. **43**, 429 (2010).
47 Y. Ge, Y. Wen, H. Liu, T. Lu, Y. Yu, X. Zhang, B. Li, S.-T. Zhang, W. Li, and B. Yang, J. Mater. Chem. C **8**, 11830 (2020).
48 D. J. Codling, G. Zheng, T. Stait-Gardner, S. Yang, M. Nilsson, and W. S. Price, J. Phys. Chem. B **117**, 2734 (2013).
49 L. Malfatti, T. Kidchob, D. Aiello, R. Aiello, F. Testa, and P. Innocenzi, J. Phys. Chem. C **112**, 16225 (2008).
50 J. Sung, P. Kim, B. Fimmel, F. Würthner, and D. Kim, Nat. Commun. **6**, 8646 (2015).
51 H. Schomburg, H. Staerk, and A. Weller, Chem. Phys. Lett. **22**, 1 (1973).
52 S. K. Rajagopal, A. R. Mallia, and M. Hariharan, Phys. Chem. Chem. Phys. **19**, 28225 (2017).
53 X. Feng, J.-Y. Hu, C. Redshaw, and T. Yamato, Chem. Eur. J. **22**, 11898 (2016).
54 A. G. Crawford, Z. Liu, I. A. I. Mkhalid, M. -H. Thibault, N. Schwarz, G. Alcaraz, A. Steffen, J. C. Collings, A. S. Batsanov, J. A. K. Howard, and T. B. Marder, Chem. Eur. J. **18**, 5022 (2012).
55 Y. Zhao and D. G. Truhlar, Theor. Chem. Acc. **120**, 215 (2008).
56 S.F. Boys and F. Bernardi, Mol. Phys. **19**, 553 (1970).
57 E. D. Glendening, C. R. Landis, and F. Weinhold, WIREs Comput. Mol. Sci. **2**, 1 (2012).
58 A. D. Hanlon and B. H. Milosavljevic, Photochem. Photobiol. Sci. **12**, 787 (2013).
59 F. V. R. Neuwahl and P. Foggi, Laser Chem. **19**, 375 (1999).
60 L. R. Williams, E. B. Gamble Jr., K. A. Nelson, S. D. Silvestri, A. M. Weiner, and E. P. Ippen, Chem. Phys. Lett. **139**, 244 (1987).
61 C. R. Goldschmidt and M. Ottolenghi, J. Phys. Chem. **74**, 2041 (1970).
62 M. F. M. Post, J. Langelaar, and J. D. W. Van Voorst, Chem. Phys. Lett. **10**, 468 (1971).
63 L. Zeiri, G. Berkovic, and Z. Ludmer, Chem. Phys. Lett. **147**, 279 (1988).
64 F. Hirayama, T. A. Gregory, and S. Lipsky, J. Chem. Phys. **58**, 4696 (1973).
65 H.-B. Lin and M. R. Topp, Chem. Phys. Lett. **48**, 251 (1977).
66 T. Itoh, Chem. Rev. **112**, 4541 (2012).
67 D. Rehm and A. Weller, Isr. J. Chem. **8**, 259 (1970).
68 P. Coppens, J. Benedict, M. Messerschmidt, I. Novozhilova, T. Graber, Y.-S. Chen, I. Vorontsov, S. Scheins, and S.-L. Zheng, Acta Cryst. **A66**, 179 (2010).
69 S. K. Brayshaw, J. W. Knight, P. R. Raithby, T. L. Savarese, S. Schiffers, S. J. Teat, J. E. Warrena, and M. R. Warren, J. Appl. Cryst. **43**, 337 (2010).
70 S. Techert, F. Schotte, and M. Wulff, Phys. Rev. Lett. **86**, 2030 (2001).
71 K. Basuroy, Y. Chen, S. Sarkar, J. Benedict, and P. Coppens, Struct. Dyn. **4**, 024501 (2017).
72 H. Liu, L. Yao, B. Li, X. Chen, Y. Gao, S. Zhang, W. Li, P. Lu, B. Yang, and Y. Ma, Chem. Comm. **52**, 7356 (2016).
73 Y. Shen, H. Liu, S. Zhang, Y. Gao, B. Li, Y. Yan, Y. Hu, L. Zhao, and B. Yang, J. Mater. Chem. C **5**, 10061 (2017).

74 W. Jiang, Y. Shen, Y. Ge, C. Zhou, Y. Wen, H. Liu, H. Liu, S. Zhang, P. Lu, and B. Yang, J. Mater. Chem. C **8**, 3367 (2020).